ZEBRAFISH
Volume 10, Number 3, 2013

DOI: 10.1089/zeb.2013.0882

Topographical Analysis of Reactive Zinc in the Central Nervous System of Adult Zebrafish (*Danio Rerio*)

Marcos M. Braga,[1,2] Denis B. Rosemberg,[1,2] Diogo L. de Oliveira,[1,2] Cássio M. Loss,[1,2] Sandro D. Córdova,[1,2] Eduardo P. Rico,[1,2] Emerson S. Silva,[1,2] Renato D. Dias,[1,2] Diogo O. Souza,[1,2] and Maria Elisa Calcagnotto[1,2]

Abstract

Reactive zinc (Zn) is crucial for neuronal signaling and is largely distributed within presynaptic vesicles of some axon terminals of distinct vertebrates. However, the distribution of reactive Zn throughout the central nervous system (CNS) is not fully explored. We performed a topographical study of CNS structures containing reactive Zn in the adult zebrafish (*Danio rerio*). Slices of CNS from zebrafish were stained by Neo-Timm and/or cresyl violet. The Zn specificity of Neo-Timm was evaluated with Zn chelants, N,N,N′,N′-Tetrakis(2-pyridylmethyl)ethylenediamine (TPEN), sodium diethyldithiocarbamate (DEDTC), Zn sulfide washing solution, and hydrochloric acid (HCl). Unfixed slices were also immersed in the fluorescent Zn probe (zinpyr-1). Yellow-to-brown-to-black granules were revealed by Neo-Timm in the zebrafish CNS. Telencephalon exhibited slightly stained regions, while rhombencephalic structures showed high levels of staining. Although stained granules were found on the cell bodies, rhombencephalic structures showed a neuropil staining profile. The TPEN produced a mild reduction in Neo-Timm staining, while HCl and mainly DEDTC abolished the staining, indicating a large Zn content. This result was also confirmed by the application of a Zn probe. The present topographical study revealed reactive Zn throughout the CNS in adult zebrafish that should be considered in future investigation of Zn in the brain on a larger scale.

Introduction

Zinc (Zn) is the second most abundant trace metal in organisms and is essential for many metalloproteins.[1,2] As a micronutrient, Zn is crucial for several cellular processes, such as defense against free radicals, immune function, cell proliferation and reproduction. Zn is an important neuromodulator at synapses of specific brain regions, for example, the hippocampus and cortex,[3,4] and it is implicated in the memory formation process.[5] Alterations in Zn levels contribute to the imbalance in neurotransmission[6] and brain hypoxia[7] that is associated with brain disorders such as seizures and neuronal injury, respectively. Thus, the cellular control of Zn levels in the central nervous system (CNS) is critical for its homeostasis.

The reactive or chelatable Zn, a pool of Zn loosely bound to biomolecules, is implicated in neuronal signaling, and it is largely distributed within presynaptic vesicles in some axon terminals.[8] Zn-containing axon terminals are distributed throughout the telencephalon and are markedly colocalized with a subset of glutamatergic neurons.[9–11] There is robust evidence that links the glutamate receptor function and excitatory amino-acid transporter 1 to the neuromodulatory activity of Zn.[6] In contrast, the role of reactive Zn in the CNS, which is present in the synaptic reorganization of Zn-containing neurons in brain disorders[12–14] and following physical training,[15] is not clear. As a consequence, chelatable Zn has been detected in the brain of distinct vertebrate classes, such as mammals,[13,14] reptiles,[16–18] birds,[19] and fish,[20] using histochemical techniques (e.g., Neo-Timm staining). However, given its ubiquitous presence, phylogenetic conservation, and plasticity, a broader screening of reactive Zn could be a useful strategy to better understand its function in the CNS. While a topographical analysis of reactive Zn throughout the CNS in mammals can be quite complex, the use of small and simple animal models could be an interesting approach to easily perform this investigation.

Zebrafish (*Danio rerio*) is an attractive animal model for neuroscience studies.[21–24] In addition to its intrinsic advantages, such as low-cost, easy maintenance, abundant offspring production,[22,25] and highly conserved genes,[26] the adult zebrafish has a CNS with fewer neurons compared to other

[1]Departamento de Bioquímica, Universidade Federal do Rio Grande do Sul, Porto Alegre, Brazil.
[2]Instituto Nacional de Ciência e Tecnologia em Excitotoxicidade e Neuroproteção (INCT-EN), Porto Alegre, Brazil.

vertebrates. This feature makes it an appropriate animal model to investigate the pool of chelatable Zn throughout the CNS. A recent study performed by Ho and colleagues[27] reported the expression of Zn transporters in the brain during development, suggesting that Zn may play an important role in this species. Moreover, the zebrafish has also been used as an emergent organism for evaluating seizures[28,29] and hypoxia/ischemia-related phenotypes,[30] two brain disorders associated with Zn dyshomeostasis. Thus, for all these features, the distribution of the chelatable form of Zn in the CNS of adult zebrafish should be evaluated.

Therefore, the goal of the present study was to investigate the distribution of reactive Zn throughout the CNS of adult zebrafish. To address this issue, we used Zn-sensitive Neo-Timm staining and optical density quantification to perform a topographical study of Neo-Timm-positive regions/areas and a cytoarchitectonic location of stained granules in whole CNS structures. Zn specificity of the Neo-Timm was also examined using Zn chelants N,N,N′,N′-Tetrakis(2-pyridylmethyl)ethylenediamine (TPEN) and sodium diethyldithiocarbamate (DEDTC), Zn sulfide washing solutions, and a membrane-permeable fluorescent Zn probe, zinpyr-1 (ZP1).

Materials and Methods

Zebrafish

Twenty-five wild-type male and female adult zebrafish (*Danio rerio*) were obtained from a specialized supplier (Delphis) and maintained under standard conditions. To neutralize ions that could be harmful to fish, we used tap water with Tetra's AquaSafe® (Tetra). The water was kept under continuous mechanical and chemical filtration at 26°C ± 2°C, and fish were housed for 2 weeks before the experiments under a 12-h light/12-h dark cycle photoperiod (lights on at 7:00 am). The animals were healthy and fed twice a day with a commercial flake fish food (Alcon Basic®). As a positive control, three Wistar rats were obtained from our animal facility.

The fish were cryoanesthetized and immediately euthanized by decapitation to remove the brain and spinal cord. The Wistar rats were euthanized by decapitation, and the brain was dissected. All animals were maintained according to the National Institute of Health Guide for the Care and Use of Laboratory Animals. The experiments were approved by the Ethics Committee of Universidade Federal do Rio Grande do Sul (number 19780–CEUA).

Neo-Timm staining

The protocol used for histochemical staining of reactive Zn was based on the traditional Neo-Timm method previously described for immersion autometallography.[31] Briefly, each zebrafish CNS was immersed in 2 mL of 3% glutaraldehyde solution in a 0.1 M phosphate buffer (pH 7.4) for 24 h, and then moved to 2 mL of a sodium sulfide solution (1% Na_2S) in a 0.12 M Millonig's buffer (97 mM NaOH, 138 mM NaH_2PO_4, and 0.18 mM $CaCl_2$) for 24 h. Later, each sample was embedded in 4% agarose (Invitrogen) and glued with cyanoacrylic adhesive to the stage of a vibroslicer (VTS-1000; Leica). Coronal (30-μm-thick) slices were cut in phosphate-buffered saline, mounted on gelatinized slides, and left to dry. For Neo-Timm staining, the CNS slices were incubated in a solution of 120 mL of 50% gum Arabic with 1.85 g of hydroquinone in 30 mL of H_2O, 5.12 g of citric acid, 4.72 g of sodium citrate in 20 mL of H_2O, and 0.17 g of silver nitrate in 1 mL of H_2O for 120 min. For topographical analysis of Neo-Timm staining in zebrafish, four adjacent series of slices were sampled from each CNS. Three series were processed using the Neo-Timm method, and the fourth was stained with cresyl violet (Nissl staining present in the cell bodies) (Supplementary Fig. S1; Supplementary Data are available online at www.liebertpub.com/zeb). For the cytoarchitectonic analysis of Neo-Timm staining, samples were cut and counterstained with both Neo-Timm and cresyl violet.[32] In addition, care was taken to verify the specificity of the Neo-Timm staining in zebrafish: (1) the CNSs were also immersed in 0.1% and 1% Na_2S, producing identical staining; (2) negative control slices (Na_2S-free) were also performed; (3) silver exposure time was also examined at 60 and 180 min, but 120 min exhibited specific staining without overexposure; (4) the rat brains were immersed in a 1% sulfide solution, similar to the method used for zebrafish, which resulted in an identical staining to that observed in perfused rodents (see Supplementary Fig. S2); (5) only ultrapure and metal-free reagents were used in the experiments.

Neo-Timm staining quantification

To define the Neo-Timm-positive regions/areas in the zebrafish CNS, we used the topographical description of zebrafish brain published by Rink and Wullimann[33] and Ullmann and colleagues.[34] The quantification of Neo-Timm staining was performed by analyzing the optical density of the total area for each CNS region in the slice under 10× magnification. The levels of optical densities were considered to determine each region according to all Neo-Timm-positive regions in the zebrafish CNS. Thus, regions with low (<17 arbitrary units), intermediate (≥17 and <34 a.u.), or high (≥34 a.u.) levels of staining were defined by the size, intensity, and number of Neo-Timm-positive granules. Regions that extended to more than one slice, received the correspondent slice number following the abbreviation (e.g., PGz_1, PGz_2). To minimize quantification error, the images were digitalized using the same parameters with a light microscope (Nikon Eclipse E-600) coupled with a camera (Nikon DXM 1200C CCD). The pictures were captured by NIS Elements AR 2.30 software (Nikon), and the images were equalized with the same contrast and brightness, and then converted to an 8-bit gray scale. The optical density was quantified using ImageJ 1.37v software. Specifically, the mean of three small squares with unspecific stain were determined for each slice as a background. This mean value was subtracted from the optical density of the total CNS areas for each slice.

Categorization of the whole Neo-Timm-positive structures

The whole CNS structures of adult zebrafish were categorized according to the level of Neo-Timm staining. The score for each structure (e.g., PGz) was determined by the mean of optical density of the correspondent CNS regions (e.g., PGz_1, $PGz_2 \ldots PGz_5$) in the same stained brain, considering three to six independent experiments. Fifty-nine anatomical structures were compared and categorized based upon high-, intermediate-, and low-level staining.

Determination of chelatable Zn specificity

To evaluate the Zn specificity in Neo-Timm staining, we used two membrane-permeable Zn chelants; TPEN (Sigma) was added in the glutaraldehyde fixative solution to a final concentration of 5 mM in 10% dimethyl sulfoxide (DMSO); and DEDTC (700 mg/kg) (Sigma) dissolved in the phosphate buffer 0.1 M (pH 7.4) was intraperitoneally injected 30 min before the Neo-Timm procedure as a previous study.[35] In parallel, we performed a pretreatment of some CNS slices with hydrochloric acid (HCl) 0.1 M for 30 min or 15% TCA for 5 min because both can dissolve Zn sulfide.[36–38] As controls, we performed three independent experiments using distinct vehicle solutions that did not alter the Neo-Timm staining pattern.

Zinpyr-1 staining procedure

The membrane-permeable fluorescent Zn probe, ZP1 (Sigma), was used as an additional technique to investigate the specificity and location of reactive Zn revealed by Neo-Timm, as previously described.[39] Briefly, adult zebrafish head were immediately frozen by burying them in dry ice for 3 min. Next, frozen samples were mounted on the chuck of a closed cabinet cryostat (Leica CM1850) and cut at −9°C to −11°C. The slices (60 μm thick) were allowed to dry on clean glass slides at room temperature for 1–2 h. The staining was achieved by applying ZP1 in DMSO dissolved in 0.9% NaCl to a final concentration of 20 μM at room temperature. After 3 min, the excess solution was removed, and the slides were viewed and photographed using a Nikon Eclipse E-600 coupled with a Nikon DXM 1200C CCD. Confocal imaging was performed using a LSM 710 Zeiss microscope, with illumination with a 488 ηm multiline argon laser and viewing through a 500 ηm long-pass filter.

Although ZP1 is considered a fluorescent probe highly specific for reactive Zn, we confirm this feature by adding TPEN on zebrafish CNS slice before ZP1 application. This approach did completely abolish ZP1 staining (see Supplementary Fig. S3).The effect of DEDTC application on the slices was similar to TPEN (data not shown). Therefore, as ZP1 is highly specific for reactive Zn, these data reinforce the strong affinity of these chelators to reactive Zn.

Results

Neo-Timm staining characterization

The Neo-Timm staining showed the presence of granules with a color variation from yellow-to-brown-to-black (bright gray-to-black in gray-scale images) and with diameters ranging from 0.5 to 4 μm thick. Overall, the granules exhibited a high staining intensity (black color) with sizes of approximately 2 μm thick, as observed in the periventricular gray zone (PGz) of the optic tectum (Fig. 1A,B).

Topographical CNS Neo-Timm staining

To evaluate the Neo-Timm staining, we divided the zebrafish CNS into three topographical sections.

Telencephalon. The most rostral section of the zebrafish brain exhibited a low level of staining, with the weakest staining and smallest number of Neo-Timm-positive granules (Fig. 2).

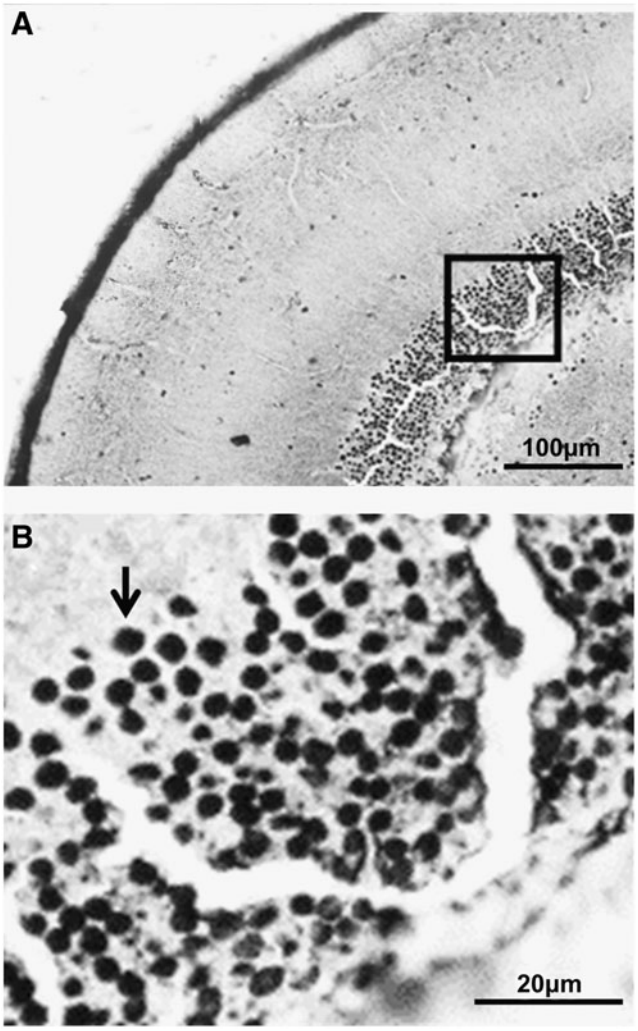

FIG. 1. Neo-Timm staining of adult zebrafish brain slice (30 μm thick). Low **(A)** and high **(B)** magnification of periventricular gray zone (PGz) of the optic tectum (OT) of adult zebrafish. The *black arrow* indicates a stained granule at higher magnification of the area denoted by the *square* in **(A)**.

Specifically, the olfactory bulb (Fig. 2A) showed small granules concentrated in the internal cellular layer (ICL) with an intermediate level of staining. Meanwhile, the glomerular layer (GL) and external cellular layer (ECL_1 and ECL_2) were weakly stained.

In the subsequent slice, we observed few widespread granules in the telencephalic hemispheres (Fig. 2B). Intermediate staining was observed in the posterior and dorsal nucleus (Dp_1 and Dd) of the dorsal area, in the anterior part of the parvocellular preoptic nucleus (PPa), and in the ventral part of the entopeduncular nucleus (NEv). Low-level staining was observed in the lateral nucleus of the dorsal telencephalic area (Dl), the dorsal part of the entopeduncular nucleus (NEd), the supracommissural nucleus of the ventral area (Vs), and the medial nucleus of the dorsal area (Dm). Additionally, the central nucleus of the dorsal area (Dc) was weakly stained, with an optical density close to the background.

In the preoptic slice (Fig. 2C), the magnocellular preoptic nucleus (PM) showed a high level of staining. The entopeduncular nucleus—ventral part (ENv), posterior part of

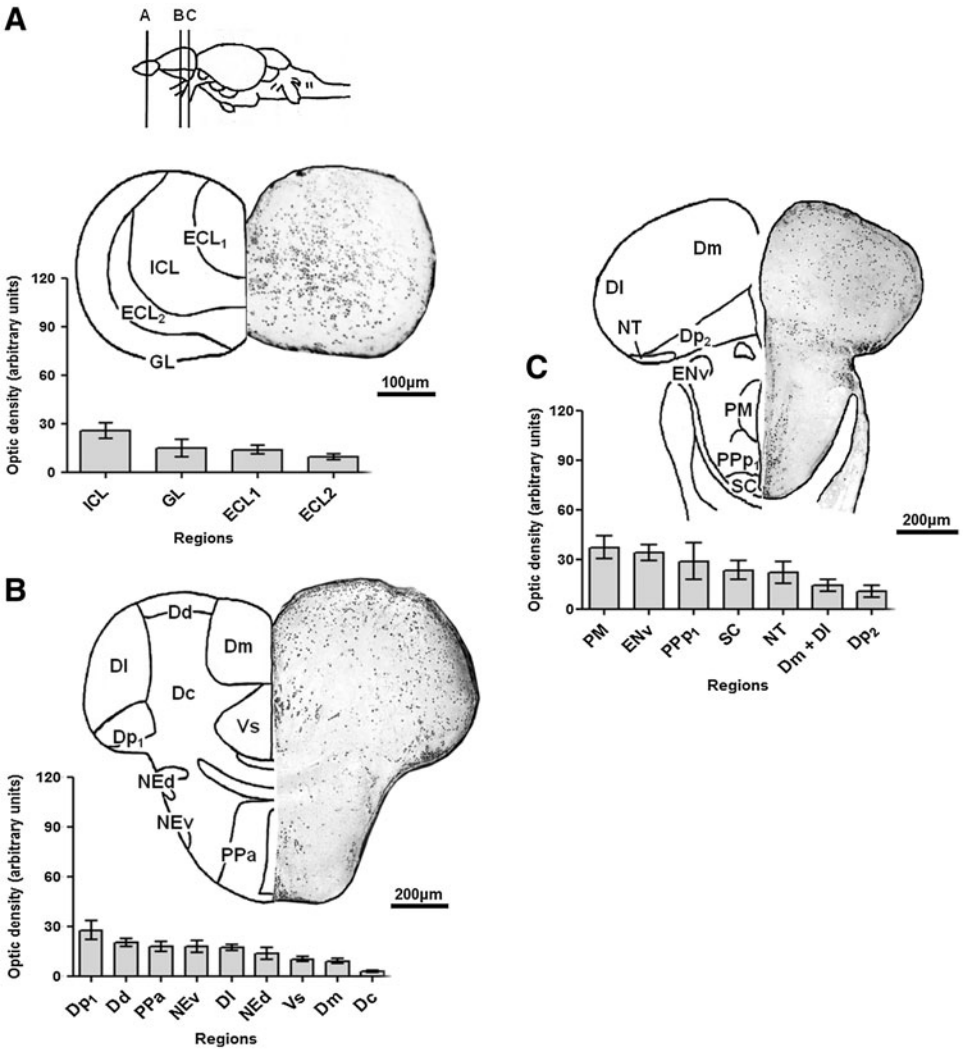

FIG. 2. Neo-Timm-positive regions: anterior central nervous system (CNS) section. Sequential representative slices (30 μm thick) showing the olfactory bulb **(A)**, telencephalon **(B)**, and preoptic **(C)** regions. The whole areas were delimited and measured in optic density. Values are presented as the mean ± SEM in arbitrary units ($n = 3$–6). For abbreviations, see Table 1. Schematic drawings adapted from a previous work.[40]

the parvocellular preoptic nucleus (PPp_1), suprachiasmatic nucleus (SC), and nucleus taeniae (NT) exhibited an intermediate staining profile. Finally, the posterior (Dp_2), medial, and lateral (Dm + Dl) nucleus of the dorsal telencephalic area exhibited a lower level of Neo-Timm staining.

Midbrain and diencephalon. At the initial portion of the diencephalon/mesencephalon (Fig. 3A), the PPp_2, anterior thalamic nucleus (A), ventromedial thalamic nucleus (VM), and ventral zone of the hypothalamic periventricular nucleus (Hv) displayed abundant Neo-Timm-positive cells. The habenula (H) and the ventrolateral optic tract (vot) exhibited an intermediate level of staining. The ventrolateral thalamus (VL) and optic tectum (OT_1) exhibited a low level of staining with few Neo-Timm granules.

In the subsequent slice (Fig. 3B), PGz_1 had markedly more Neo-Timm-positive granules (high optical density) than surrounding regions. The periventricular nucleus of the posterior tuberculum (PTp), torus longitudinalis (TL_1), and subcommissural nucleus (SCN) also had many Neo-Timm-positive granules, but exhibited an intermediate level of staining. The mesencephalic nucleus of the trigeminal nerve (MNV), ventral part of the periventricular pretectal nucleus (PPv), torus lateralis (TLa_1), and OT_2 had a lower level staining.

In the third slice (Fig. 3C), the granular layer in the lateral part of the valvula cerebelli (Val), the dorsal tegmental nucleus (DTN_1), PGz_2, and the central preglomerular nucleus (PGc) exhibited high levels of staining. An intermediate level of Neo-Timm staining was detected in the TL_2, dorsal zone of the hypothalamic periventricular nucleus (Hd_1), and OT_3. In contrast, a low level of staining was observed in the central and diffuse nucleus of the hypothalamic inferior lobe (CIL + DIL), corpus mamillare (CM_1), TLa_2, ventrolateral ($TSvl_1$), and central (TSc_1) nucleus of the torus semicircularis.

In the last representative slice of this segment (Fig. 3D), we observed a high optical density in the TL_3, PGz_3, Hd_2, granular layer of the lateral and medial part (Val + Vam) of the valvula cerebelli, CM_2, and perilemniscal nucleus (PL). The oculomotor nucleus (NIII), DTN_2, and OT_4 had intermediate levels of staining. Finally, few granules were found in the nucleus lateralis valvulae (NLV), nucleus of the lateral lemniscus (NLL), TSc_2, and $TSvl_2$, resulting in regions with a low level of staining.

Hindbrain: rostral part. This segment delimits the rhombencephalic region, which exhibited significant Neo-Timm staining.

In the first slice, the PGz_4, central gray (CG), and corpus cerebelli (CCe_1) (Fig. 4A) were highly stained regions. An

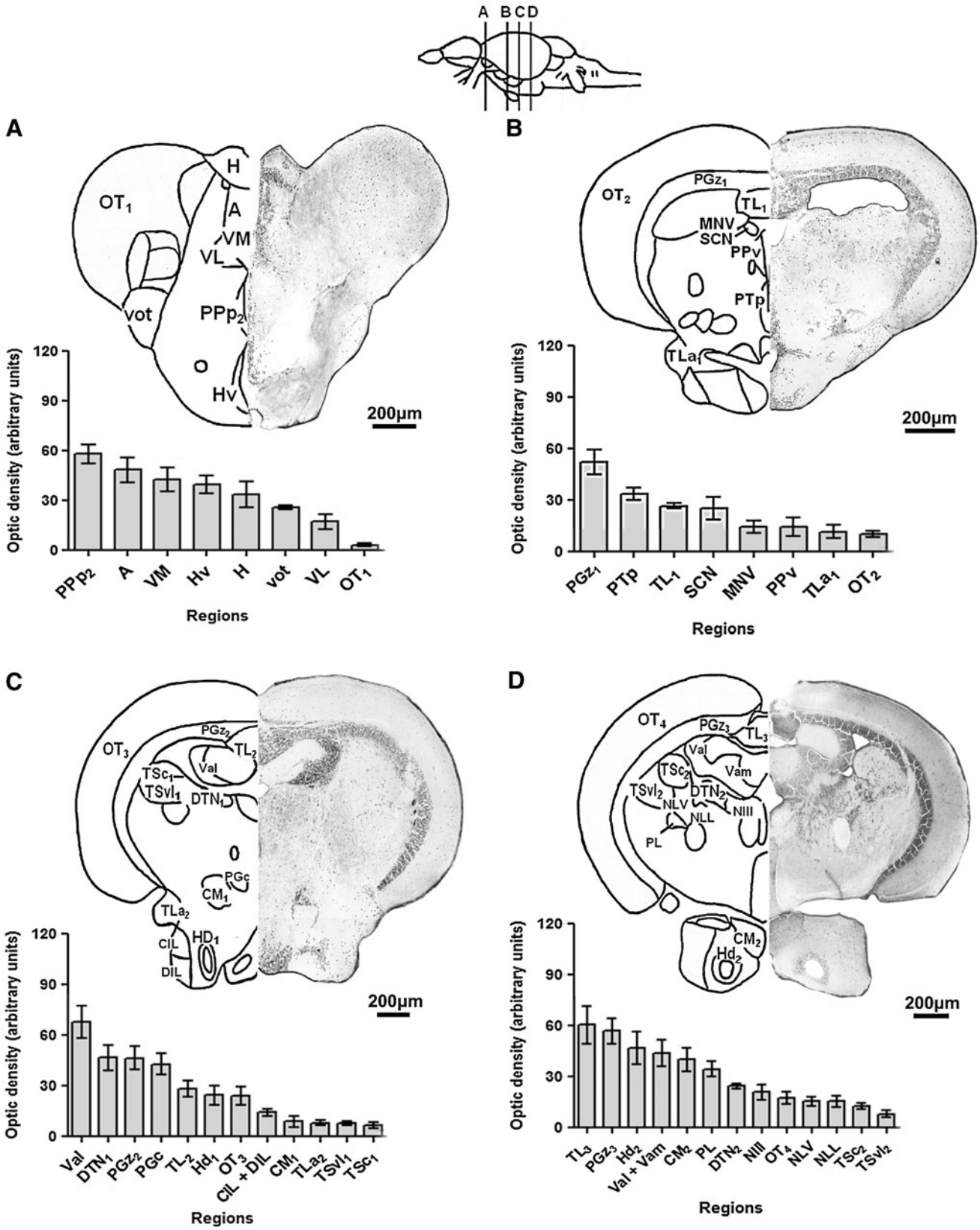

FIG. 3. Neo-Timm-positive regions: middle CNS section. Sequential representative slices (30 μm thick) showing the diencephalon/mesencephalon **(A–D)** regions. The whole areas were delimited and measured in optic density. Values are presented as the mean ± SEM in arbitrary units ($n = 3$–6). For abbreviations, see Table 1. Schematic drawings adapted from a previous work.[40]

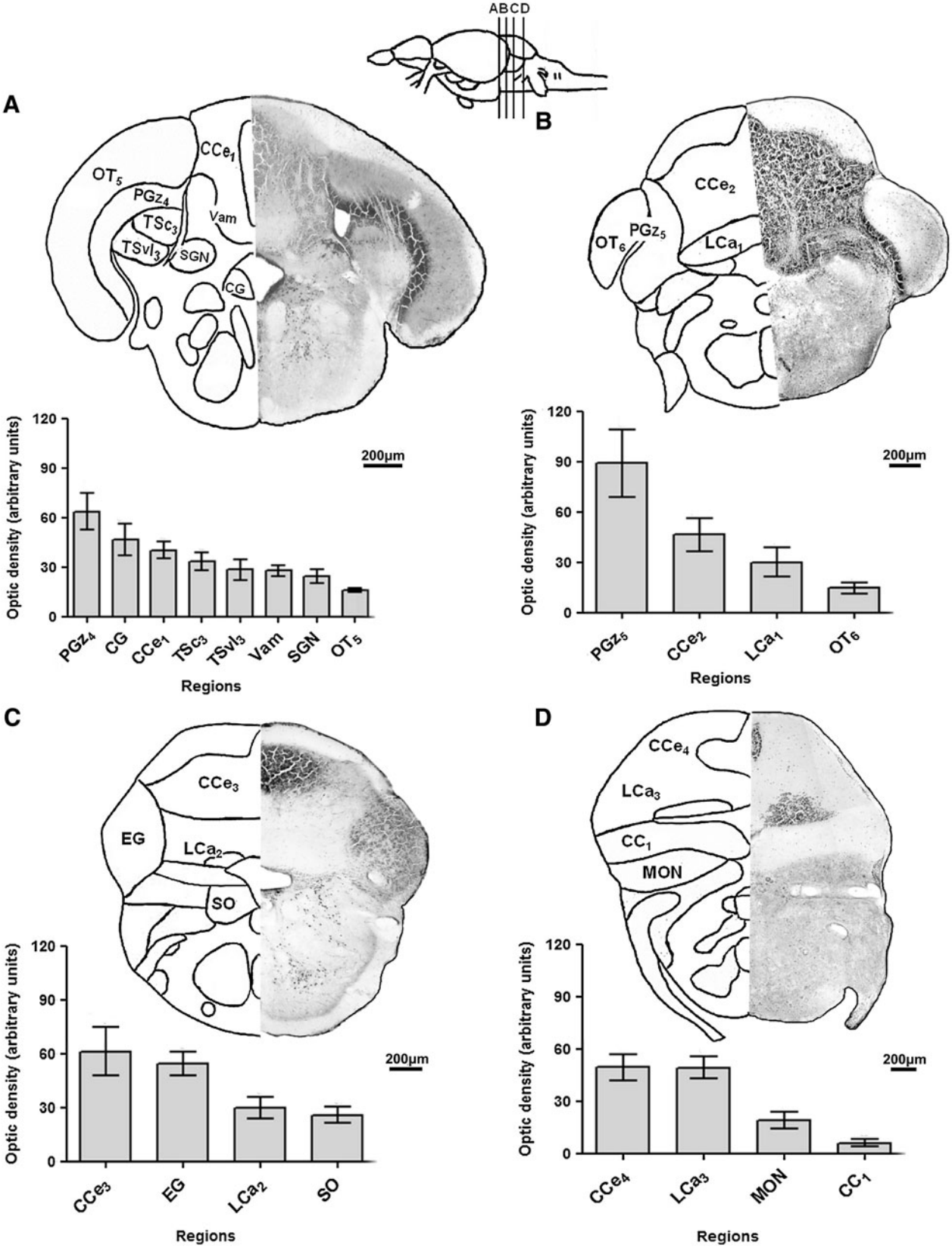

FIG. 4. Neo-Timm-positive regions: posterior CNS section—rostral rhombencephalon. Sequential representative slices (30 μm thick) showing rostral rhombencephalon **(A–D)** regions. The whole areas were delimited and measured by optic density. Values are presented as the mean ± SEM in arbitrary units ($n = 3$–6). For abbreviations, see Table 1. Schematic drawings adapted from a previous work.[40]

intermediate level of staining was observed in the TSc_3, $TSvl_3$, Vam, and secondary gustatory nucleus (SGN), while the OT_5 had a low level of staining.

In the subsequent topographical slice (Fig. 4B), we detected the highest level of Neo-Timm staining in the final portion of PGz_5 when compared with the other CNS regions. Likewise, the CCe_2 also exhibited a high level of staining. In parallel, intermediate and low levels of staining were observed in the lobus caudalis cerebelli (LCa_1) and the OT_6, respectively.

Positive staining was found in four specific regions on the next representative slice (Fig. 4C). A high level of staining was found in the CCe_3 and eminentia granularis (EG), while LCa_2 and the secondary octaval population (SO) had an intermediate level of staining.

In the next slice (Fig. 4D), a considerable number of Neo-Timm-positive granules were concentrated in the CCe_4 and LCa_3, representing highly stained regions. On the other hand, the medial octavolateral nucleus (MON) and the crista cerebellaris (CC_1) had intermediate and low levels of staining, respectively.

Hindbrain: caudal part. In the representative caudal slice of rhombencephalon (Fig. 5A), the glossopharyngeal lobe (LIX) exhibited a high level of staining. An intermediate level of staining was observed in the facial lobe (LVII), and low levels were observed in the CC_2.

In the spinal cord (Fig. 5B), few positive granules were observed. The ventral part of the lateral funiculus (Flv) and the ventral funiculus (Fv) exhibited only an intermediate optical density value. Additionally, low levels of staining were found in the ventral horn (VH) and the dorsal part of the lateral funiculus (Fld).

From this entire topographical analysis, we observed higher levels of Neo-Timm staining in the hindbrain (predominantly in the rhombencephalon) followed by midbrain/diencephalon and telencephalon sections of the zebrafish CNS.

The whole Neo-Timm-positive structures of adult zebrafish CNS

The rhombencephalic (Val, CG, EG, Vam, LIX, LCa, and CCe) and the diencephalic/mesencephalic structures (PGz, A, TL, Hv, PGc, VM, Hd, DTN, and PL) exhibited a high level of Neo-Timm staining. The preoptic zone displayed few structures with a high level of staining, and only PPp and PM had a substantial optical density (Table 1).

Throughout the zebrafish CNS, we observed structures with intermediate levels of staining such as in the diencephalon/mesencephalon (H, PTp, CM, vot, NIII, VL, and SCN) and in the rhombencephalon (SO, SGN, MON, LVII, and NLL). Similarly, the telencephalon exhibited a considerable number of structures with an intermediate optical density (ICL, Dp, NEv, Dd, PPa, and ECL). The preoptic zone represented by ENv, SC, and NT also had intermediate levels of Neo-Timm staining. In addition, the spinal cord exhibited structures with intermediate levels of staining, such as the Flv and Fv (Table 1).

The group with a low level of staining comprised mostly of telencephalic (Dl, GL, Dm, NEd, Vs, and Dc) and diencephalic/mesencephalic structures (TSvl, DIL, CIL, NLV, OT, MNV, PPv, TSc, and TLa). Moreover, lower levels of Neo-

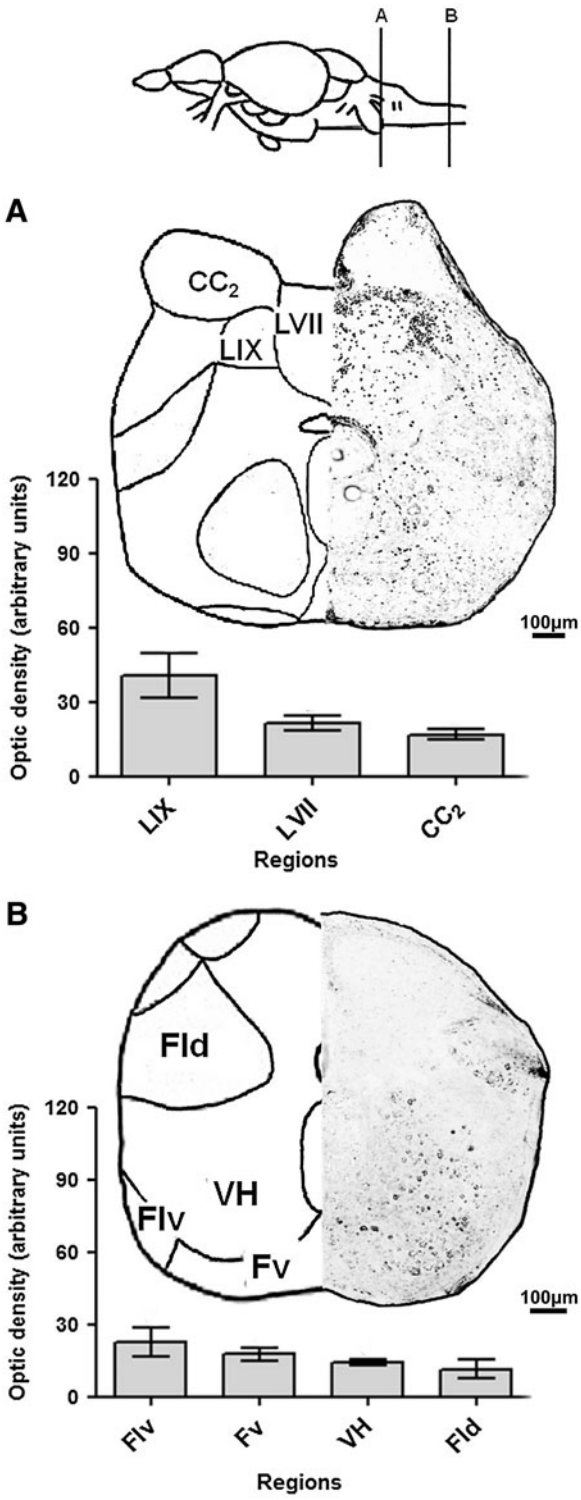

FIG. 5. Neo-Timm-positive regions: posterior CNS section—caudal rhombencephalon and spinal cord. Sequential representative slices (30 μm thick) showing caudal rhombencephalon **(A)** and spinal cord **(B)** regions. The whole areas were delimited and measured in optic density. Values are presented as the mean ± SEM in arbitrary units ($n = 3$–6). For abbreviations, see Table 1. Schematic drawings adapted from a previous work.[40]

Table 1. Neo-Timm Staining in Zebrafish Central Nervous System Structures

Staining level	*Structures*	*Abbreviations*	*Optic density*[a]
High	Valvula cerebelli, lateral part (granular layer)	Val	58.60 ± 6.14
	Central gray	CG	53.25 ± 9.26
	Periventricular gray zone of the optic tectum	PGz	50.80 ± 4.31
	Eminentia granularis	EG	48.79 ± 3.81
	Anterior thalamic nucleus	A	48.23 ± 7.54
	Torus longitudinalis	TL	45.57 ± 6.75
	Ventral zone of the hypothalamic periventricular nucleus	Hv	44.49 ± 2.91
	Central preglomerular nucleus	PGc	42.66 ± 6.08
	Ventromedial thalamic nucleus	VM	42.41 ± 7.13
	Dorsal zone of the hypothalamic periventricular nucleus	Hd	41.45 ± 4.87
	Valvula cerebelli, medial part (granular layer)	Vam	41.07 ± 2.60
	Glossopharyngeal lobe	LIX	40.62 ± 8.81
	Posterior part of the parvocellular preoptic nucleus	PPp	39.75 ± 3.38
	Dorsal tegmental nucleus	DTN	39.59 ± 3.20
	Perilemniscal nucleus	PL	38.38 ± 1.94
	Magnocellular preoptic nucleus	PM	37.20 ± 6.89
	Lobus caudalis cerebelli	Lca	37.11 ± 3.86
	Corpus cerebelli	Cce	35.62 ± 2.50
Intermediate	Entopeduncular nucleus, ventral part	Env	33.99 ± 4.68
	Habenula	H	33.22 ± 8.10
	Periventricular nucleus of the posterior tuberculum	PTp	30.19 ± 1.86
	Secondary octaval population	SO	29.56 ± 3.81
	Corpus mamillare	CM	28.23 ± 4.65
	Secondary gustatory nucleus	SGN	27.65 ± 3.93
	Medial octavolateral nucleus	MON	26.76 ± 1.75
	Ventrolateral optic tract	Vot	25.75 ± 1.07
	Internal cellular layer	ICL	25.53 ± 4.81
	Oculomotor nucleus	NIII	24.37 ± 2.85
	Suprachiasmatic nucleus	SC	23.38 ± 5.64
	Ventral part of the lateral funiculus	Flv	22.56 ± 6.02
	Nucleus taeniae	NT	22.09 ± 6.57
	Posterior nucleus of the dorsal Telencephalic area	Dp	21.89 ± 2.67
	Ventrolateral thalamic nucleus	VL	20.90 ± 2.33
	Ventral part of the entopeduncular nucleus	Nev	20.61 ± 2.48
	Dorsal nucleus of the dorsal telencephalic area	Dd	20.24 ± 2.43
	Anterior part of the parvocellular preoptic nucleus	Ppa	20.18 ± 2.38
	Subcommissural nucleus	SCN	19.09 ± 3.87
	Facial lobe	LVII	18.85 ± 1.45
	Nucleus of the lateral lemniscus	NLL	18.08 ± 2.54
	Ventral funiculus	Fv	17.56 ± 2.46
	External cellular layer	ECL	17.55 ± 2.18
Low	Ventrolateral nucleus of the torus semicircularis	TSvl	16.74 ± 2.72
	Diffuse nucleus of the hypothalamic inferior lobe	DIL	15.78 ± 2.02
	Central nucleus of the hypothalamic inferior lobe	CIL	15.78 ± 2.02
	Nucleus lateralis valvulae	NLV	15.33 ± 2.73
	Lateral nucleus of the dorsal telencephalic area	Dl	15.16 ± 2.11
	Glomerular layer	GL	14.90 ± 5.32
	Optic tectum	OT	14.94 ± 1.56
	Mesencephalic nucleus of the trigeminal nerve	MNV	14.22 ± 3.75
	Ventral horn	VH	14.21 ± 1.13
	Ventral part of the periventricular pretectal nucleus	PPv	14.02 ± 5.42
	Central nucleus of the torus semicircularis	TSc	12.36 ± 2.21
	Dorsal part of the lateral funiculus	Fld	11.38 ± 4.06
	Crista cerebellaris	CC	11.36 ± 1.83
	Medial nucleus of the dorsal telencephalic area	Dm	11.06 ± 2.14
	Dorsal part of the entopeduncular nucleus	Ned	10.50 ± 1.79
	Supracommissural nucleus of the telencephalic ventral area	Vs	10.18 ± 1.48
	Torus lateralis	Tla	7.05 ± 1.11
	Central nucleus of the dorsal telencephalic area	Dc	2.75 ± 0.51

Values are presented as mean ± SEM in arbitrary units ($n = 3–6$).

[a]Mean optical density of the correspondent CNS regions (e.g., PGz1, PGz2…PGz5) in the same stained brain, considering three to six independent experiments.

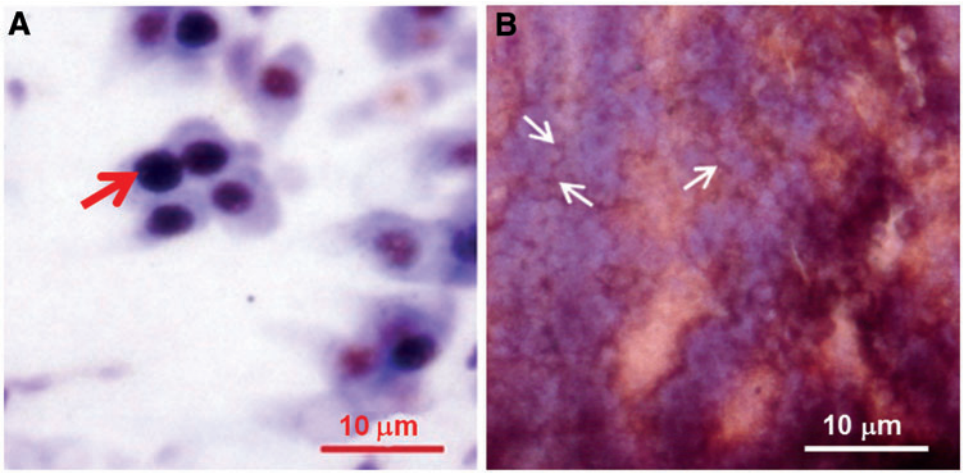

FIG. 6. Cytoarchitectonic distribution of Neo-Timm staining. Note that Neo-Timm staining is indicated by *arrows*. Counterstaining with cresyl violet and Neo-Timm revealed positive granules on the cell body **(A)** and in neuropil **(B)** as stained in central nucleus of the dorsal telencephalic area (Dc) and in torus longitudinalis (TL), respectively. Color images available online at www.liebertpub.com/zeb

Timm staining were found in structures of the rhombencephalon (CC) and spinal cord (VH and Fld) (Table 1).

Cytoarchitectonic distribution of Neo-Timm staining

To evaluate the cytoarchitectonic distribution of Neo-Timm granules, slices from zebrafish CNS were counterstained with Neo-Timm and cresyl violet. As a result, we observed two distinct Neo-Timm-positive areas, which were found on the cell bodies and in the neuropil of the zebrafish CNS.

Neo-Timm-stained granules were found on the cell bodies, mainly in the telencephalon. Structures with this pattern of staining were observed in the Dc (Fig. 6A), CG, PGz, A, Hv, PGc, VM, Hd, PPp, H, PL, PM, ENv, PTp, SO, SGN, MON, vot, ICL, NIII, SC, Flv, NT, Dp, VL, NEv, Dd, PPa, SCN, Fv, ECL, DIL, CIL, Dl, GL, VH, PPv, Fld, CC, Dm, NEd, Vs, TLa, Dc, LIX, DTN, LVII, TSvl, NLV, OT, MNV, and TSc.

Other structures exhibited Neo-Timm staining in the neuropil. In fact, this staining profile was mainly observed in rhombencephalic structures in the hindbrain, such as Val, EG, Vam, LIX, LCa, CCe, and LVII. Similar staining was also found in the TL (Fig. 6B), DTN, CM, NLL, TSvl, NLV, MNV, and TSc.

Neo-Timm staining attributed to chelatable Zn

To identify the contribution of chelatable Zn in Neo-Timm staining, we used, TPEN and DEDTC, two strong Zn chelants; HCl or TCA, which dissolve Zn sulfide (Fig. 7).

The pretreatment with TPEN produced a mild reduction in Neo-Timm staining in zebrafish CNS when compared with

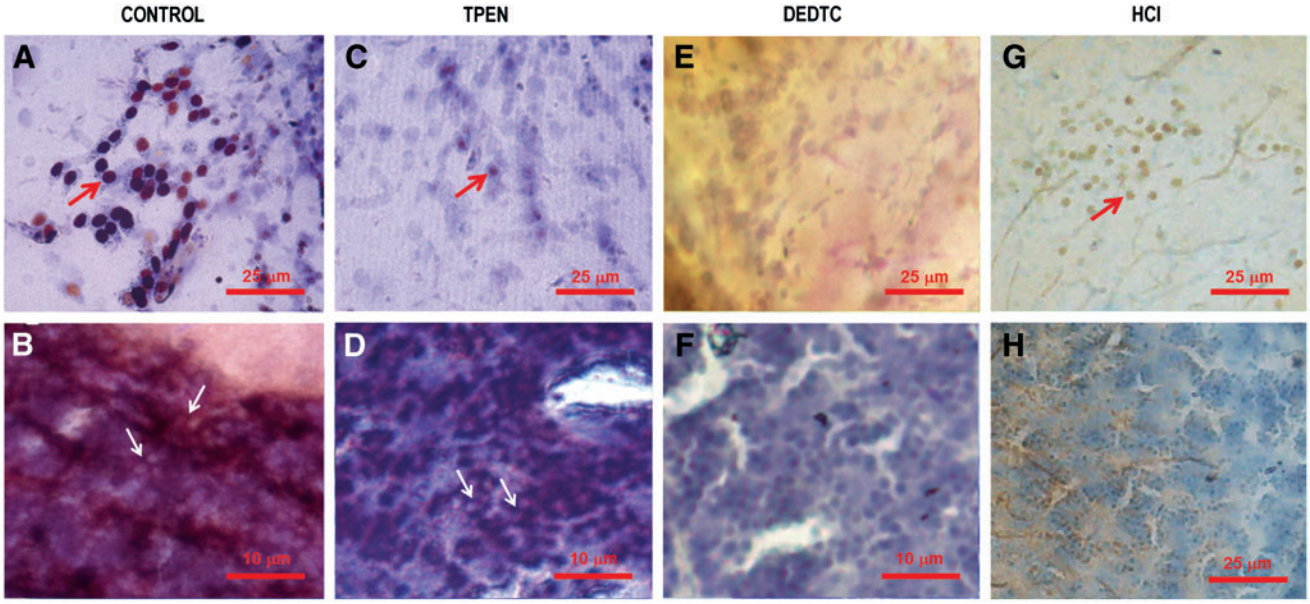

FIG. 7. Chelatable Zn present in Neo-Timm staining. The Neo-Timm staining is indicated by *arrows*. Neo-Timm and cresyl *violet* counterstaining of the central nucleus of the dorsal telencephalic area (Dc) **(A)** and valvula cerebelli, lateral part (Val) **(B)** of controls. Note that pretreatment with 5 mM TPEN decreased the Neo-Timm staining on the cell bodies in the Dc **(C)** and slightly reduced positive granules in neuropil regions, for example, in the Val **(D)**. Administration i.p. of DEDTC 700 mg/kg did completely abolish the *silver* staining on the cell bodies **(E)** and in neuropil regions **(F)**. The use of 0.1 M HCl in the preparation of the slices did significantly reduce Neo-Timm staining on the cell bodies and in neuropil regions, as observed in the Dc **(G)** and Val **(H)**, respectively. Color images available online at www.liebertpub.com/zeb

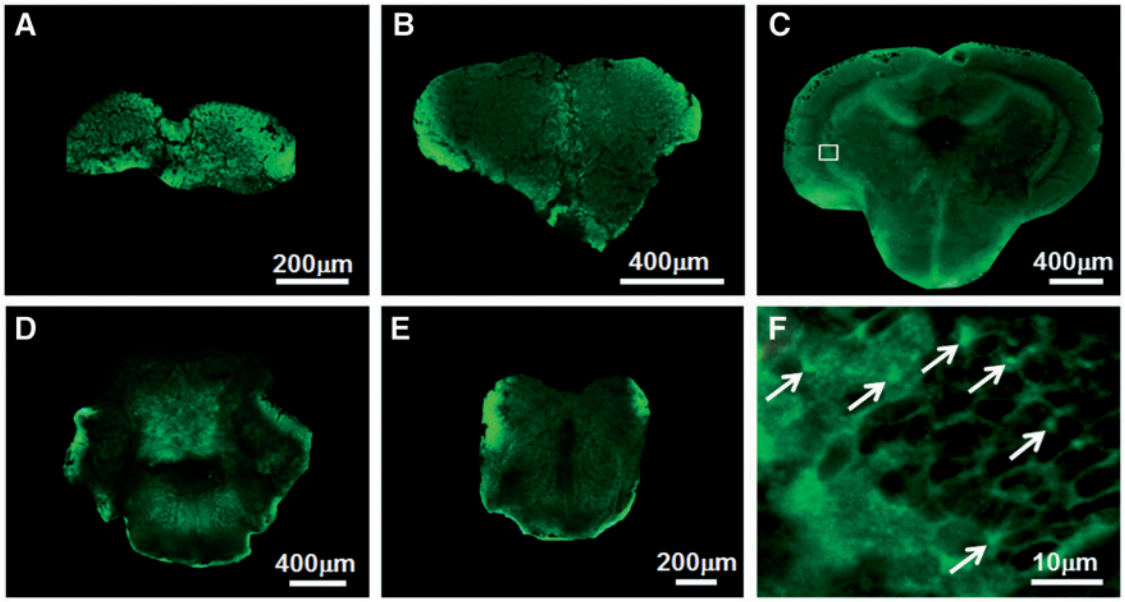

FIG. 8. Unfixed coronal slices (60 μm thick) of CNS stained by ZP1. ZP1 staining yielded widespread bright puncta in the same regions/areas of the zebrafish CNS stained by Neo-Timm. Fluorescence images of the olfactory bulb **(A)**, telencephalon **(B)**, optic tectum **(C)**, the cerebellum **(D)**, and spinal cord **(E)** showing the fluorescent staining in the representative slices. Confocal image of the periventricular gray zone (PGz) **(F)** depicted in the *box* in **(C)**. Note the distinct bright puncta (*arrows*) and the negative staining for somata, similar to those of rodents.[39] Unspecific staining is observed at the edge of the slices. Color images available online at www.liebertpub.com/zeb

the control (Fig. 7A, B). As observed in the central nucleus of the dorsal telencephalic area (Dc) in the telencephalon (Fig. 7C), TPEN decreased Neo-Timm granules located on the cell bodies. In addition, few modifications were detected in neuropil regions after TPEN administration, as seen in rhombencephalic structures, such as Val (Fig. 7D). In contrast, i.p. administration of DEDTC did completely abolish the staining on the cell bodies and in the neuropil, as showed in Dc (Fig. 7E) and Val (Fig. 7F), respectively.

The administration of TCA abolished Neo-Timm staining on the cell bodies in the telencephalon, and few alterations were observed in the staining pattern of the neuropil region in rhombencephalic structures (data not shown). Finally, HCl strikingly decreased Neo-Timm staining on the cell bodies and in neuropil regions, as indicated for the telencephalic (Fig. 7G) and rhombencephalic structures (Fig. 7H), respectively.

Zinpyr-1 staining

The ZP1 staining in the adult zebrafish CNS showed reactive Zn in all regions/areas (Fig. 8A–E) that were positive for Neo-Timm. The olfactory bulb (Fig. 8A) and spinal cord (Fig. 8E) exhibited few and widespread fluorescent staining. Similarly, the whole telencephalon was barely stained by ZP1, as in the central nucleus of the dorsal telencephalic area (Dc) (Fig. 8B). However, in the lateral nucleus of the dorsal telencephalic area (Dl), in the posterior nucleus of the dorsal telencephalic area (Dp_1), and in the supracommissural nucleus of the telencephalic ventral area (Vs), we observed some reactive Zn content. In contrast, representative slices from the optic tectum in the midbrain (Fig. 8C) and cerebellum in the hindbrain (Fig. 8D) showed regions with abundant reactive Zn content, coinciding with those obtained by Neo-Timm staining. Indeed, the periventricular gray zone of the optic tectum (PGz_3), the valvula cerebelli, lateral and medial part (Val + Vam), in the optic tectum, and corpus cerebelli (CCe_2) and lobus caudalis cerebelli (LCa_1), in the cerebellum, presented intensely fluorescent ZP1 staining.

The location of reactive Zn stained with ZP1 was determined by confocal analysis. Throughout the adult zebrafish CNS, ZP1 staining always appeared as bright puncta out of the perikarya in areas with Neo-Timm granules on the cell bodies (e.g., PGz_3 in Fig. 8F) and in regions with a neuropil staining pattern. Thus, we confirmed the result for the substantial reactive Zn content stained by Neo-Timm.

Discussion

The main finding of this study was the heterogeneous pattern of Neo-Timm staining detected for chelatable Zn in different regions and structures throughout the CNS of adult zebrafish. In distinct animal models, such as rodents, this method has been used to stain neuropil in hippocampal areas containing high levels of reactive Zn.[41] In the present study, we used Zn chelant treatments, Zn sulfide washing solutions, and a fluorescent Zn probe as approaches to support the highly specific avidity of Neo-Timm staining for reactive Zn. The use of these strategies allowed us to observe the presence of reactive Zn more predominantly in the rhombencephalon than in telencephalic structures.

As in zebrafish, the Neo-Timm method stained distinct CNS areas. We showed its specificity to reveal regions containing Zn by different approaches. In fact, the administration of TPEN, a specific Zn chelant,[42,43] produced a mild decrease of Neo-Timm-positive granules on the cell bodies and in the neuropil, suggesting the presence of reactive Zn in Neo-Timm-stained zebrafish CNS. Importantly, we cannot rule out that the residual Neo-Timm-positive granules left by TPEN

could be attributed to the nonsaturable chelant concentration or even to other metals. Indeed TPEN (5 mM) may have been insufficient to fully wash chelatable Zn from the tissue, similar to the results observed in rodents treated with the other Zn chelant.[35] Since copper and iron may be revealed by Neo-Timm,[44] these metals could also explain the residual staining observed in the zebrafish CNS. However, the marked absence of positive granules after the i.p. injection of DEDTC and the administration of Zn sulfide washing solutions,[36–38] suggests that other metals have a negligible contribution to Neo-Timm staining in the adult zebrafish CNS. Additionally, the presence of reactive Zn detected by Neo-Timm staining was reinforced by ZP1 application, which demonstrated that chelatable Zn was found at similar CNS regions and structures stained by Neo-Timm. Thus, as for other animal models,[39,45,46] the use of a fluorescent Zn probe in the zebrafish CNS confirmed the high specificity of Neo-Timm for the detection of reactive Zn.

The cytoarchitectonic distribution of reactive Zn in the zebrafish CNS detected by counterstaining of cresyl violet/Neo-Timm is consistent with the findings in other animal models.[13,14,20,47] Although we observed a pattern of staining in the neuropil that is usually seen in rodent hippocampi, the zebrafish CNS also exhibited Neo-Timm-positive granules located within the limits of the cell bodies, which could be either inside or surrounding the soma. Interestingly, Pinuela and colleagues[20] also found Neo-Timm staining on the cell bodies in the rainbow trout brain, possibly representing axosomatic terminals. However, it is also known that the presence of Neo-Timm granules in the healthy perikarya of mammals represents unspecific staining because chelating agents are unable to clean positive granules.[48] Surprisingly, when we pretreated the brains with Zn chelants before Neo-Timm staining, the granules on the cell bodies were also suppressed. It is difficult to know whether these granules correspond to those stained in the neuropil of mammals, which are correlated with the pool of reactive Zn located inside the vesicles of excitatory synapses. Future ultrastructural studies of Neo-Timm staining using zebrafish could be an interesting strategy to clarify the exact subcellular location of reactive Zn in regions with granules in the neuropil and areas on the cell bodies. Nevertheless, taking into account the confocal analysis of ZP1 staining, the reactive Zn was detected outside cell bodies throughout the zebrafish CNS, similar to rodents.[39]

Because our data support the presence of an abundant reactive Zn content in the adult zebrafish CNS, the whole structures were categorized according to the level of staining. As described, structures with a high level of Neo-Timm staining were predominantly found in the rhombencephalon in the hindbrain, similar to Zn-containing neurons in the hippocampal region of distinct vertebrate classes.[13,14,16–19] As in other teleosts, zebrafish also present the lateral nucleus of the dorsal telencephalic area (Dl), located in the pallium region of CNS, which structurally corresponds to the hippocampus.[49] Similar to a previous study using rainbow trout perfused with 1% sulfide,[20] our data showed less reactive Zn in the telencephalon when compared with other parts of the CNS of adult zebrafish. These results confirm the phylogenetic trend of the translocation of a high level of Neo-Timm from the rhombencephalon in zebrafish to telencephalic structures in mammals, reptiles, and birds. Although, further studies are required to elucidate this hypothesis, a small amount of reactive Zn in the zebrafish telencephalon could be sufficient to perform an allosteric modulation, like in mammals.[50,51]

It is well known that the abundant reactive Zn stained by Neo-Timm in the rodent hippocampus is associated with learning and memory formation[5] because Zn acts as a neuromodulator colocalized in vesicles with glutamate in Zn-containing neurons.[3] In fact, the corelease of reactive Zn and glutamate has been observed at the synaptic terminals of rod photoreceptors in zebrafish, modulating the synaptic activity.[52] Interestingly, we have observed a high level of Zn stained by Neo-Timm in the rhombencephalic structures (Val, CG, EG, Vam, LCa, and CCe), which are known to exhibit an abundant distribution of glutamatergic neurons.[53] These results lead us to hypothesize an important role of reactive Zn in the rhombencephalon of zebrafish as a neuromodulator in structures responsible for movement control.[54] As observed in rodents,[48] the substantial reactive Zn detected by Neo-Timm staining in the thalamic structures (A and VM) could also act in the control of the multifunctional thalamic and hypothalamic nucleus in the zebrafish CNS. Currently, we can only speculate on the neuromodulatory action of reactive Zn detected by Neo-Timm, and further studies must be performed to clarify the neurochemical function of reactive Zn in the CNS of zebrafish.

In summary, our data suggest that the zebrafish CNS contains a considerable amount of reactive Zn with a heterogenic distribution, as detected by Neo-Timm staining and a fluorescent Zn probe. Although, the rhombencephalic structures of zebrafish had higher levels of Neo-Timm staining than the telencephalon, the cytoarchitectonic location of the granules seemed to be similar to other vertebrates. Because this topographical investigation showed reactive Zn throughout the adult zebrafish CNS, additional studies could help to understand the exact function of the Zn content, mainly in those structures with high staining levels. Moreover, we described, for the first time, a protocol for assessing the chelatable Zn pool in the zebrafish CNS using ZP1 staining in unfixed brain slices. This protocol, together with Neo-Timm staining, could be a valuable tool for additional studies that aim to evaluate the functional roles of Zn. Therefore, considering the widespread distribution of reactive Zn and the possibility for testing the whole zebrafish CNS in topographical analyses, these techniques could be considered in future research to clarify the mechanisms underlying Zn homeostasis in the CNS of vertebrates on a larger scale.

Acknowledgments

We are grateful to Henrique Biehl from the Centro de Microscopia Eletrônica (CME) of the Universidade Federal do Rio Grande do Sul for the confocal technical assistance.

Disclosure Statement

No competing financial interests exist.

References

1. Vallee BL, Auld DS. Zinc coordination, function and structure of zinc enzymes and other proteins. Biochemistry 1990;29:5647–5659.

2. Braga MM, Dick T, de Oliveira DL, Guerra AS, Leite MC, Ardais AP, *et al.* Cd modifies hepatic Zn deposition and modulates δ-ALA-D activity and MT levels by distinct mechanisms. J Appl Toxicol 2012;32:20–25.
3. Qian J, Noebels JL. Exocytosis of vesicular zinc reveals persistent depression of neurotransmitter release during metabotropic glutamate receptor long-term depression at the hippocampal CA3-CA1 synapse. J Neurosci 2006;26: 6089–6095.
4. Cunningham MG, Ames HM, Christensen MK, Sorensen JC. Zincergic innervation of medial prefrontal cortex by basolateral projection neurons. Neuroreport 2007;18:531–535.
5. Sindreu C, Storm DR. Modulation of neuronal signal transduction and memory formation by synaptic zinc. Front Behav Neurosci 2011;5:68.
6. Paoletti P, Vergnano AM, Barbour B, Casado M. Zinc at glutamatergic synapses. Neuroscience 2009;158:126–136.
7. Stork CJ, Li YV. Rising zinc: a significant cause of ischemic neuronal death in the CA1 region of rat hippocampus. J Cereb Blood Flow Metab 2009;29:1399–1408.
8. Frederickson CJ, Suh SW, Silva D, Thompson RB. Importance of zinc in the central nervous system: the zinc-containing neurons. J Nutr 2000;130:1471–1483.
9. Martinez-Guijarro FJ, Soriano E, Del Rio JÁ, Lopez-Garcia C. Zinc-positive boutons in the cerebral cortex of lizards show glutamate immunoreactivity. J Neurocytol 1991;20:834–843.
10. Beaulieu C, Dyck R, Cynader M. Enrichment of glutamate in zinc-containing terminals of the cat visual cortex. Neuroreport 1992;3:861–864.
11. Sindreu CB, Varoqui H, Erickson JD, Perez-Clausell J. Boutons containing vesicular zinc define a subpopulation of synapses with low AMPAR content in rat hippocampus. Cereb Cortex 2003;13:823–829.
12. Penkowa M, Moos T. Disruption of the blood-brain interface in neonatal rat neocortex induces a transient expression of metallothionein in reactive astrocytes. Glia 1995;13:217–227.
13. Garcia-Cairasco N, Wakamatsu H, Oliveira JA, Gomes EL, Del Bel EA, Mello LE. Neuroethological and morphological (Neo-Timm staining) correlates of limbic recruitment during the development of audiogenic kindling in seizure susceptible Wistar rats. Epilepsy Res 1996;26:177–192.
14. Chakravarty DN, Babb TL, Chung CK, Mikuni N. Bilateral kainic acid lesions in the rat hilus induce non-linear additive mossy fiber neoinnervation. Neurosci Lett 1997;230:175–178.
15. Toscano-Silva M, Silva SG, Scorza FA, Bonvent JJ, Cavalheiro EA, Arida RM. Hippocampal mossy fiber sprouting induced by forced and voluntary physical exercise. Physiol Behav 2010;101:302–308.
16. Perez-Clausell J. The organization of zinc-containing terminal fields in the brain of the lizard Podarcis hispanica. A histochemical study. J Comp Neurol 1988;267:153–171.
17. Smeets WJAJ, Perez-Clausell J, Geneser FA. The distribution of zinc in the forebrain and midbrain of the lizard Gekko gecko. A histochemical study. Anat Embryol 1989;180:45–56.
18. Pimentel HC, dos Santos JR, Macedo-Lima M, de Almeida FT, Santos ML, Molowny A, *et al.* Structural organization of the cerebral córtex of the neotropical lizard Tropidurus hispidus. Cell Tissue Res 2011;343:319–330.
19. Faber H, Braun K, Zuschratter W, Scheich H. System specific distribution of zinc in the chick brain. A light- and electron-microscopic study using the Timm method. Cell Tissue Res 1989;258:247–257.
20. Pinuela C, Baatrup E, Geneser FA. Histochemical distribution of zinc in the brain of the rainbow trout, Oncorhynchos myciss. I. The telencephalon. Anat Embryol 1992;185:379–388.
21. Senger MR, Rosemberg DB, Rico EP, de Bem Arizi M, Dias RD, Bogo MR, *et al. In vitro* effect of zinc and cadmium on acetylcholinesterase and ectonucleotidase activities in zebrafish (Danio rerio) brain. Toxicol In Vitro 2006;20:954–958.
22. Egan RJ, Bergner CL, Hart PC, Cachat JM, Canavello PR, Elegante MF, *et al.* Understanding behavioral and physiological phenotypes of stress and anxiety in zebrafish. Behav Brain Res 2009;205:38–44.
23. Gerlai R. Using zebrafish to unravel the genetics of complex brain disorders. Curr Top Behav Neurosci 2012;12:3–24.
24. Rosemberg DB, Braga MM, Rico EP, Loss CM, Córdova SD, Mussulini BH, *et al.* Behavioral effects of taurine pretreatment in zebrafish acutely exposed to ethanol. Neuropharmacology 2012;63:613–623.
25. Gerlai R, Lee V, Blaser R. Effects of acute and chronic ethanol exposure on the behavior of adult zebrafish (Danio rerio). Pharmacol Biochem Behav 2006;85:752–761.
26. Barbazuk WB, Korf I, Kadavi C, Heyen J, Tate S, Wun E, *et al.* The syntenic relationship of the zebrafish and human genomes. Genome Res 2000;10:1351–1358.
27. Ho E, Dukovcic S, Hobson B, Wong CP, Miller G, Hardin K, *et al.* Zinc transporter expression in zebrafish (Danio rerio) during development. Comp Biochem Physiol C Toxicol Pharmacol 2012;155:26–32.
28. Baraban SC, Taylor MR, Castro PA, Baier H. Pentylenetetrazole induced changes in zebrafish behavior, neural activity and c-fos expression. Neuroscience 2005;131:759–768.
29. Alfaro JM, Ripoll-Gomez J, Burgos JS. Kainate administered to adult zebrafish causes seizures similar to those in rodent models. Eur J Neurosci 2011;33:1252–1255.
30. Zakhary SM, Ayubcha D, Ansari F, Kamran K, Karim M, Leheste JR, *et al.* A behavioral and molecular analysis of ketamine in zebrafish. Synapse 2011;65:160–167.
31. Danscher G, Stoltenberg M, Bruhn M, Sondergaard C, Jensen D. Immersion autometallography: histochemical *in situ* capturing of zinc ions in catalytic zinc–sulfur nanocrystals. J Histochem Cytochem 2004;52:1619–1625.
32. Wullimann MF, Puelles L. Postembryonic neural proliferation in the zebrafish forebrain and its relationship to prosomeric domains. Anat Embryol 1999;199:329–348.
33. Rink E, Wullimann MF. Connections of the ventral telencephalon (subpallium) in the zebrafish (Danio rerio). Brain Res 2004;1011:206–220.
34. Ullmann JFP, Cowin G, Kurniawan ND, Collin SP. A three-dimensional digital atlas of the zebrafish brain. Neuroimage 2010;51:76–82.
35. Foresti ML, Arisi GM, Fernandes A, Tilelli CQ, Garcia-Cairasco N. Chelatable zinc modulates excitability and seizure duration in the amygdale rapid kindling model. Epilepsy Res 2008;79:166–172.
36. Kozma M, Szerdahelyi P, Kasa P. Histochemical detection of zinc and copper in various neurons of the central nervous system. Acta Histochem 1981;69:12–17.
37. Szerdahelyi P, Kasa P. Histochemical demonstration of copper in normal rat brain and spinal cord. Evidence of localization in glial cells. Histochemistry 1986;85:341–347.
38. Danscher G. The autometallographic zinc-sulphide method. A new approach involving *in vivo* creation of nanometer-sized zinc sulphide crystal lattices in zinc-enriched synaptic and secretory vesicles. Histochem J 1996;28:361–373.
39. Frederickson CJ, Burdette SC, Frederickson CJ, Sensi SL, Weiss JH, Yin HZ, *et al.* Method for identifying cells

suffering toxicity by use of a novel fluorescent sensor. J Neurosci Methods 2004;139:79–89.
40. Clemente D, Porteros A, Weruaga E, Alonso JR, Arenzana FJ, Aijón J, *et al.* Cholinergic elements in the zebrafish central nervous system: histochemical and immunohistochemical analysis. J Comp Neurol 2004;474:75–107.
41. Perez-Clausell J, Danscher G. Intravesicular localization of zinc in rat telencephalic boutons. A histochemical study. Brain Res 1985;337:91–98.
42. Medvedeva YV, Lin B, Shuttleworth W, Weiss JH. Intracellular Zn2+ accumulation contributes to synaptic failure, mitochondrial depolarization, and cell death in acute slice oxygen-glucose deprivation model if ischemia. J Neurosci 2009;29:1105–1114.
43. Xu Z, Yoon J, Spring DR. Fluorescent chemosensors for Zn(2+). Chem Soc Rev 2010;39:1996–2006.
44. Danscher G. Histochemical demonstration of heavy metals. A revised version of the sulphide silver method suitable for both light and electron microscopy. Histochemistry 1981; 71:1–16.
45. Birinyi A, Parker D, Antal M, Shupliakov O. Zinc co-localizes with GABA and glycine in synapses in the lamprey spinal cord. J Comp Neurol 2001;433:208–221.
46. Varea E, Ponsoda X, Molowny A, Danscher G, Lopez-Garcia C. Imaging synaptic zinc release in living nervous tissue. J Neurosci Methods 2001;110:57–63.
47. Lopez-Garcia C, Varea J, Palop JJ, Nacher J, Ramirez C, Ponsoda X, *et al.* Cytochemical techniques for zinc and heavy metals localization in nerve cells. Micros Res Tech 2002;56:318–331.
48. Mengual E, Casanovas-Aguilar C, Perez-Clausell J, Gimenez-Amaya JM. Thalamic distribution of zinc-rich terminal fields and neurons of origin in the rat. Neuroscience 2001;102:863–884.
49. Mueller T, Dong Z, Berberoglu MA, Guo S. The dorsal pallium in zebrafish, *Danio rerio* (Cyprinidae, Teleostei). Brain Res 2011;1381:95–105.
50. Mony L, Kew JN, Gunthorpe MJ, Paoletti P. Allosteric modulators of NR2B-containing NMDA receptors: molecular mechanisms and therapeutic potential. Br J Pharmacol 2009;157:1301–1317.
51. Paoletti P. Molecular basis of NMDA receptor functional diversity. Eur J Neurosci 2011;33:1351–1365.
52. Redenti S, Ripps H, Chappell RL. Zinc release at the synaptic terminals of rod photoreceptors. Exp Eye Res 2007;85:580–584.
53. Bae YK, Kani S, Shimizu T, Tanabe K, Nojima H, Kimura Y, *et al.* Anatomy of zebrafish cerebellum and screen for mutations affecting its development. Dev Biol 2009;330: 406–426.
54. Ito M. Control of mental activities by internal models in the cerebellum. Nat Rev Neurosci 2008;9:304–313.

Address correspondence to:
Marcos Martins Braga, MSc
Departamento de Bioquímica
Instituto de Ciências Básicas da Saúde
Universidade Federal do Rio Grande do Sul
Rua Ramiro Barcelos 2600-Anexo
Porto Alegre 90035-000, RS
Brazil

E-mail: marcosmbraga@gmail.com